Available online at www.sciencedirect.com
SCIENCE DIRECT®
ELSEVIER
Solid-State Electronics 48 (2004) 1325–1335
SOLID-STATE ELECTRONICS
www.elsevier.com/locate/sse

Monte Carlo modeling of the electron mobility in strained $Si_{1-x}Ge_x$ layers on arbitrarily oriented $Si_{1-y}Ge_y$ substrates

S. Smirnov *, H. Kosina

Institute for Microelectronics, TU Vienna, Gusshausstrasse 27-29/E360, A-1040 Vienna, Austria

Received 5 November 2003; received in revised form 24 December 2003; accepted 30 January 2004
Available online 13 April 2004

The review of this paper was arranged by Prof. C.K. Maiti

Abstract

Under strain the electronic properties of Si and SiGe significantly change. For the semiconductor industry the improvement of the kinetic properties is most interesting. In this work we present Monte Carlo modeling of the low field electron mobility in strained $Si_{1-x}Ge_x$ layers grown on relaxed $Si_{1-y}Ge_y$ substrates of arbitrary orientation. An analytical conduction band model is used. The valley splitting is calculated using linear deformation-potential theory. The dependence on the substrate orientation is taken into consideration by transforming the strain tensor. Hooke's law is then used to determine the elements of the strain tensor in the principle coordinate system. The phonon and ionized impurity scattering rates are modified to account for the change of the conduction band. A zero field Monte Carlo method used to calculate the low field mobility tensor in the strained material is described and the influence of the Pauli exclusion principle is discussed. Simulation results are given for both undoped and doped layers for different compositions x and y as well as for several substrate orientations. The anisotropic behavior of the mobility as a function of the in-plane angle is demonstrated and the interplay between the strain effects and effects due to Fermi–Dirac statistics is shown.
© 2004 Elsevier Ltd. All rights reserved.

1. Introduction

With each new technology generation geometric scaling has become an increasingly complex and expensive task. An additional way to improve device performance is to enhance the carrier transport by changing the material properties. In advanced semiconductor devices strain can be used as an additional degree of freedom to enhance transport properties due to band structure changes. A dominant change is the degeneracy reduction of the conduction band extrema which are degenerate in a relaxed material because of the symmetry of the crystal. Physical modeling is necessary because the kinetic processes in semiconductors have a complex behavior which cannot be described analytically. Furthermore strain affects the kinetic properties of the material in a rather complicated manner.

One possible way of describing the kinetic properties of a material is given by the semiclassical Boltzmann kinetic equation. This is an integral–differential equation which becomes nonlinear if the quantum mechanical Pauli exclusion principle is taken into account. There are various analytical and numerical approaches for the solution of this equation. However, only the Monte Carlo approach allows comprehensive physical models to be included without further approximations. Especially strain effects can be included naturally in the formalism provided by the Boltzmann equation. Both analytical and full band structures can be taken into account by the Monte Carlo approach. The full band analysis of strained Si and SiGe grown on relaxed [0 0 1]

* Corresponding author. Tel.: +43-1-58801-36016; fax: +43-1-58801-36099.
E-mail address: kosina@iue.tuwien.ac.at (H. Kosina).

0038-1101/$ - see front matter © 2004 Elsevier Ltd. All rights reserved.
doi:10.1016/j.sse.2004.01.014

substrates has been performed in [1]. However, strained layers grown on substrates with other orientations and the influence of ionized impurity scattering have not been considered. In [2] the Ridley model has been employed for strained doped layers but, the effect of the Pauli exclusion principle has been neglected.

In this work we investigate the low field electron mobility. Thus an analytical model for the band structure including an anisotropic effective mass and a nonparabolicity correction [3] is used here:

$$\epsilon(\mathbf{k})(1+\alpha\epsilon(\mathbf{k})) = \frac{\hbar}{2}\left(\frac{k_x^2}{m_x}+\frac{k_y^2}{m_y}+\frac{k_z^2}{m_z}\right). \quad (1)$$

The influence of strain on the kinetics is studied using a zero field Monte Carlo method. For the electron gas in doped layers degenerate statistics is considered and the scattering operator accounts for the Pauli principle.

The paper is organized as follows. In Section 2 the splitting of the conduction band in strained SiGe is described for the X and L valleys. A general substrate orientation is taken into account. In Section 3 the scattering rates of the dominant processes are modified to account for the change of the conduction band. In Section 4 the zero field Monte Carlo method used is presented. Simulation results are discussed in Section 5 and some concluding remarks are drawn in Section 6.

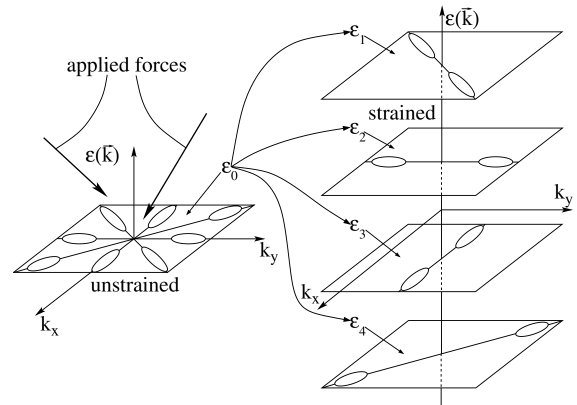

Fig. 1. Full reduction of degeneracy due to the applied stress for a hypothetical band structure. For a general orientation of applied forces $\varepsilon_1 \neq \varepsilon_2 \neq \varepsilon_3 \neq \varepsilon_4$.

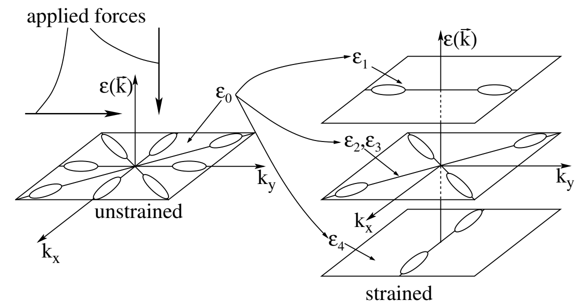

Fig. 2. Partial reduction of degeneracy due to the applied stress for a hypothetical band structure. Applied forces are oriented along a high symmetry axes: $\varepsilon_1 \neq \varepsilon_2 = \varepsilon_3 \neq \varepsilon_4$.

2. Conduction band in strained SiGe

Linear deformation-potential theory is used to calculate the splitting of the conduction band minima in strained SiGe. This theory has been first justified within the effective mass approximation by Bardeen and Shockley [4] and is thus commonly referred to as the Bardeen–Shockley theory. Originally this theory has been applied to study the electron interaction with acoustic phonons and later to formulate the theory of strained materials. Within this theory an energy extremum is expanded into a Taylor series in powers of a quantity characterizing the strength of the lattice strain. The expansion is truncated after the first power of this parameter, resulting in a linear the theory. Neglecting terms of the second order is equivalent to the effective masses being unchanged by the induced strain.

As Si and Ge have their conduction band extrema at quasi-momenta $\mathbf{k} \neq 0$, the applied stress reduces the original degeneracy of band states with different quasi-momenta. This reduction depends on the relative orientation of the quasi-momentum for a given conduction band extremum and the applied forces, as schematically illustrated in Figs. 1 and 2. For a general orientation of applied forces all band extrema can be split. However if forces are applied along some high symmetry axes the degeneracy reduction can be partial. Extrema are forming subsets within which the degeneracy is conserved, but extrema from different subsets are no longer degenerate.

In $Si_{1-x}Ge_x$ layers grown on relaxed $Si_{1-y}Ge_y$ substrates stress due to lattice mismatch always arises when the Ge compositions are different, $x \neq y$. The direction and the magnitude of the applied forces in such a system depend on the orientation of the $Si_{1-y}Ge_y$ substrate and the Ge compositions x and y. This stress leads to a deformation of the perfect crystal. It is assumed that the thickness is below the critical value which implies absence of dislocations. As a result the degeneracy of the conduction band is reduced. The splitting of the conduction band minima has a strong impact on the transport properties of strained SiGe active layers in comparison with unstrained ones. In particular it causes anisotropy of transport quantities such as electron mobility. For Si, Ge and SiGe the low field electron mobility is represented by a scalar, that is, the mobility tensor is diagonal with equal diagonal elements. In the strained layer the diagonal elements are in general dif-

ferent. The difference of the kinetic properties for different orientations can be significant and can be used to optimize the characteristics of advanced semiconductor devices.

2.1. Energy shift

As it has been pointed out above in a strained solid the energy of an extremum is expanded into the Taylor series in powers of some small quantity characterizing the strength of the lattice strain. For weak strain it is natural to perform the expansion in powers of the strain tensor components around the unstrained point. The energy shift of the kth nondegenerate band extremum is in general expressed as:

$$\Delta\epsilon^{(k)} = \sum_{ij} \Xi_{ij}^{(k)} \varepsilon_{ij}. \quad (2)$$

The coefficients of this expansion form a second rank tensor called the deformation potential tensor. This tensor is a characteristic of a given nondegenerate band of a solid. Due to the symmetry property of the strain tensor the deformation potential tensor is also symmetric:

$$\Xi_{ij}^{(k)} = \Xi_{ji}^{(k)}. \quad (3)$$

Such tensor has only six independent components. For cubic crystals the number of independent components reduces to three, denoted as Ξ_{u}, Ξ_{d} and Ξ_{p}.

2.1.1. Shift of conduction band minima

In this work the X and L valleys of Si, Ge, and SiGe are considered. The symmetry of these valleys further reduces the number of independent components of the deformation potential tensor to two, namely Ξ_{u} and Ξ_{d}. The deformation potential Ξ_{d} relates to pure dilatation while Ξ_{u} is associated with a pure shear involving a uniaxial stretch along the major axis plus a symmetrical compression along the minor axis [5].

Linear deformation-potential theory implies that for conduction band extrema not located in the center of the Brillouin zone the shape of the equal energy surface does not change to the first order in strain. However, a particular extremum of the conduction band shifts under strain. The shift depends on the magnitude of applied forces and their orientation with respect to the quasi-momentum of a given extremum. The degenerate extrema are in general split. This splitting is completely determined by the deformation potentials Ξ_{d} and Ξ_{u}.

The general form of the energy shift (2) of valley i of type $k = X, L$ for an arbitrary homogeneous deformation can be written in the following form [6]:

$$\Delta\epsilon_{\mathrm{c}}^{(i,k)} = \Xi_{\mathrm{d}}^{(k)} Tr(\hat{\boldsymbol{\varepsilon}}) + \Xi_{\mathrm{u}}^{(k)} \mathbf{a}_i^T \hat{\boldsymbol{\varepsilon}} \mathbf{a}_i, \quad (4)$$

where $\mathbf{a}_i$ is a unit vector parallel to the $\mathbf{k}$ vector of valley i. From (4) it follows that degeneracy is reduced by shear strain.

2.1.2. Shift of the mean energy

The shift of the mean energy of the conduction band extrema of type k is expressed as:

$$\Delta\epsilon_{\mathrm{c,av}}^{(k)} = \left(\Xi_{\mathrm{d}}^{k} + \frac{1}{3}\Xi_{\mathrm{u}}^{k}\right) Tr(\hat{\boldsymbol{\varepsilon}}). \quad (5)$$

This shift can become important when more than one type of valley is taken into account as in general the deformation potentials Ξ_{d} and Ξ_{u} have different values for different valley types. The relative shift of the mean energy for valleys of different type can cause a repopulation between these valleys as schematically shown in Fig. 3 for the case of X and L valleys. Expression (5) is derived as an average of particular shifts given by (4). Thus some valleys of a given type can still significantly move which will cause a repopulation between particular extrema of different type while the transitions between other extrema will be reduced.

2.2. Strain tensor in the interface coordinate system

The energy splitting and the hydrostatic shift of the mean energy depend on the orientation of the applied forces. In the case of strained SiGe active layers grown on relaxed SiGe substrates this orientation is determined by the orientation of a substrate.

The interface coordinate system is specified as a system with its z-axis perpendicular to the hetero-interface. The form of the strain tensor $\hat{\boldsymbol{\varepsilon}}'$ in this coordinate system can be found as follows.

The condition of biaxial dilatation or contraction gives:

$$\varepsilon_{11}' = \varepsilon_{22}' = \varepsilon_{\parallel}, \quad (6)$$

where $\varepsilon_{\parallel}$ is the in-plane strain given as the relative lattice mismatch:

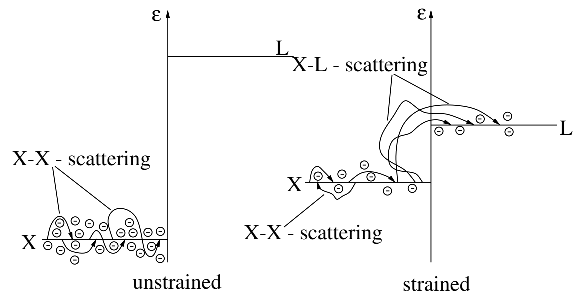

Fig. 3. Repopulation effect between X and L valleys in a strained material.

$$\varepsilon_{\parallel} = \frac{a_s - a_l}{a_l}. \tag{7}$$

Here a_l is the lattice constant of the layer and a_s that of the substrate. The substrate is assumed to be thick enough to remain unstrained. Further, the condition of vanishing in-plane shear implies:

$$\varepsilon'_{12} = 0. \tag{8}$$

It is also assumed that there is no any film distortion which means the following conditions:

$$\varepsilon'_{13} = \varepsilon'_{23} = 0. \tag{9}$$

$$\widehat{U}(\alpha,\beta,\gamma) = \begin{pmatrix} \cos\alpha\cos\beta\cos\gamma - \sin\alpha\sin\gamma & -\cos\alpha\cos\beta\sin\gamma - \sin\alpha\cos\gamma & \cos\alpha\sin\beta \\ \sin\alpha\cos\beta\cos\gamma + \cos\alpha\sin\gamma & -\sin\alpha\cos\beta\sin\gamma + \cos\alpha\cos\gamma & \sin\alpha\sin\beta \\ -\sin\beta\cos\gamma & \sin\beta\sin\gamma & \cos\beta \end{pmatrix}. \tag{14}$$

This is justified for the case of substrates with high rotational symmetry. In other cases it is relatively weak for SiGe structures.

Thus under these conditions the strain tensor for the SiGe active layer is diagonal in the interface coordinate system. The two diagonal elements are known to be equal to $\varepsilon_{\parallel}$. To determine the third diagonal element Hooke's law is applied. It linearly relates the components of the stress and the strain tensors σ_{ik} and ε_{jl}:

$$\sigma'_{\alpha\beta} = c'_{\alpha\beta ij}\varepsilon'_{ij}, \tag{10}$$

where c_{ijkl} is a tensor of rank four called the elastic stiffness tensor. As the only external stress is in-plane, the out-of-plane component will vanish

$$\sigma'_{33} = 0, \tag{11}$$

which gives for the third diagonal component of the strain tensor:

$$\varepsilon'_{33} = -\frac{c'_{3311} + c'_{3322}}{c'_{3333}}\varepsilon_{\parallel}. \tag{12}$$

2.3. Coordinate system transformation

To find the components of the elastic stiffness tensor it is necessary to perform a coordinate transformation.

2.3.1. Euler's angles

The angles which specify the relative orientation of the two coordinate systems are called Euler's angles. They are defined by the following rules. First a clockwise rotation around the z-axis is performed. This angle is usually denoted as α. Then a clockwise rotation around the new y-axis follows. This second angle is denoted as β. Finally, a clockwise rotation around the new z-axis finishes the transformation. The last angle is denoted as γ. The range of these angles are determined as follows:

$$\begin{aligned} &0 \leqslant \alpha \leqslant 2\pi, \\ &0 \leqslant \beta \leqslant \pi, \\ &0 \leqslant \gamma \leqslant 2\pi. \end{aligned} \tag{13}$$

2.3.2. Transformation operator

The transformation operator describing three successive rotations with the Euler angles α, β and γ is given as a product of three rotations and takes the following form:

Due to the symmetry property (6) the transformed strain tensor will not depend on γ. So γ is arbitrary and can be set to zero. The transformation operator takes the final form:

$$\widehat{U}(\alpha,\beta) = \begin{pmatrix} \cos\alpha\cos\beta & -\sin\alpha & \cos\alpha\sin\beta \\ \sin\alpha\cos\beta & \cos\alpha & \sin\alpha\sin\beta \\ -\sin\beta & 0 & \cos\beta \end{pmatrix}. \tag{15}$$

2.3.3. Tensor transformations

Using the transformation operator $\widehat{U}(\alpha,\beta)$ the strain tensor elements are transformed as follows:

$$\varepsilon'_{\alpha\beta} = U_{i\alpha}U_{j\beta}\varepsilon_{ij}. \tag{16}$$

Therefore the main task is to determine the elements of the strain tensor in the interface coordinate system. The strain tensor elements in the principle coordinate system are then obtained as:

$$\varepsilon_{\alpha\beta} = U_{\alpha i}U_{\beta j}\varepsilon'_{ij}. \tag{17}$$

The elastic stiffness tensor is transformed analogously:

$$c'_{\alpha\beta\delta\gamma} = U_{i\alpha}U_{j\beta}U_{k\delta}U_{l\gamma}c_{ijkl}. \tag{18}$$

2.4. Strain tensor elements in the principle coordinate system

Due to the cubic symmetry of Si and Ge there are only three nonzero components of the elastic stiffness tensor namely c_{11}, c_{12} and c_{44} in the short-hand notation [7]. This fact allows to significantly simplify the calculations of ε'_{33} which are given below for the three substrate orientations [0 0 1], [1 1 0] and [1 1 1]. The calculations for an arbitrary substrate orientation are performed in the same manner. For these three substrate orientations the transformation operator takes the form:

$$\widehat{U}_{(0\,0\,1)} = \begin{pmatrix} 1 & 0 & 0 \\ 0 & 1 & 0 \\ 0 & 0 & 1 \end{pmatrix}, \tag{19}$$

$$\widehat{U}_{(1\,1\,0)} = \begin{pmatrix} 0 & -\frac{1}{\sqrt{2}} & \frac{1}{\sqrt{2}} \\ 0 & \frac{1}{\sqrt{2}} & \frac{1}{\sqrt{2}} \\ -1 & 0 & 0 \end{pmatrix}, \tag{20}$$

$$\widehat{U}_{(1\,1\,1)} = \begin{pmatrix} \frac{1}{\sqrt{6}} & -\frac{1}{\sqrt{2}} & \frac{1}{\sqrt{3}} \\ \frac{1}{\sqrt{6}} & \frac{1}{\sqrt{2}} & \frac{1}{\sqrt{3}} \\ \sqrt{\frac{2}{3}} & 0 & \frac{1}{\sqrt{3}} \end{pmatrix}. \tag{21}$$

Using (18) and (12) one obtains:

$$\varepsilon_{33}^{\prime(0\,0\,1)} = -\frac{2c_{12}}{c_{11}}\varepsilon_{\parallel}, \tag{22}$$

$$\varepsilon_{33}^{\prime(1\,1\,0)} = -\frac{c_{11}+3c_{12}-2c_{44}}{c_{11}+c_{12}+2c_{44}}\varepsilon_{\parallel}, \tag{23}$$

$$\varepsilon_{33}^{\prime(1\,1\,1)} = -\frac{2c_{11}+4c_{12}-4c_{44}}{c_{11}+2c_{12}+4c_{44}}\varepsilon_{\parallel}. \tag{24}$$

Now the transformation of the strain tensor according to (17) gives for the elements of the strain tensor in the principle coordinate system the following expressions.

[0 0 1]:

$$\begin{aligned} &\varepsilon_{11}^{(0\,0\,1)} = \varepsilon_{22}^{(0\,0\,1)} = \varepsilon_{\parallel}, \\ &\varepsilon_{33}^{(0\,0\,1)} = -\frac{2c_{12}}{c_{11}}\varepsilon_{\parallel}, \\ &\varepsilon_{12}^{(0\,0\,1)} = \varepsilon_{13}^{(0\,0\,1)} = \varepsilon_{23}^{0\,0\,1} = 0. \end{aligned} \tag{25}$$

[1 1 0]:

$$\begin{aligned} &\varepsilon_{11}^{(1\,1\,0)} = \varepsilon_{22}^{(1\,1\,0)} = \frac{2c_{44}-c_{12}}{c_{11}+c_{12}+2c_{44}}\varepsilon_{\parallel}, \\ &\varepsilon_{33}^{(1\,1\,0)} = \varepsilon_{\parallel}, \\ &\varepsilon_{12}^{(1\,1\,0)} = -\frac{c_{11}+2c_{12}}{c_{11}+c_{12}+2c_{44}}\varepsilon_{\parallel}, \\ &\varepsilon_{13}^{(1\,1\,0)} = \varepsilon_{23}^{(1\,1\,0)} = 0. \end{aligned} \tag{26}$$

[1 1 1]:

$$\begin{aligned} &\varepsilon_{11}^{(1\,1\,1)} = \varepsilon_{22}^{(1\,1\,1)} = \varepsilon_{33}^{(1\,1\,1)} = \frac{4c_{44}}{c_{11}+2c_{12}+4c_{44}}\varepsilon_{\parallel}, \\ &\varepsilon_{12}^{(1\,1\,1)} = \varepsilon_{13}^{(1\,1\,1)} = \varepsilon_{23}^{(1\,1\,1)} = -\frac{c_{11}+2c_{12}}{c_{11}+2c_{12}+4c_{44}}\varepsilon_{\parallel}. \end{aligned} \tag{27}$$

2.5. Band structure of strained SiGe layers

Within linear deformation-potential theory only shift of valleys is taken into account whereas their shape is unchanged. This shift is described by general expressions (4) and (5). These expressions are used to calculate the energy splitting and the shift of the mean energy of the X and L valleys for the three most important substrate orientations. Generalization for the case of an arbitrary substrate orientation is straightforward.

2.5.1. Hydrostatic strain

Expression (5) gives the hydrostatic shift of the mean energy of both X and L valleys:

$$\Delta\epsilon_{\mathrm{c,av}}^{X,L} = \left(\Xi_{\mathrm{d}}^{X,L} + \frac{1}{3}\Xi_{\mathrm{u}}^{X,L}\right)(\varepsilon_{11}+\varepsilon_{22}+\varepsilon_{33}). \tag{28}$$

Note that the deformation potentials for X and L valleys are different.

2.5.2. Uniaxial strain

The splitting of equivalent valleys is given by the difference of (4) and (5) and depend on both valley type and substrate orientation.

Splitting of the X Valleys. For [0 0 1] and [1 1 0] substrates the splitting is given as:

$$\begin{aligned} &\Delta\epsilon^{(1\,0\,0)} = \Delta\epsilon^{(0\,1\,0)} = \frac{1}{3}\Xi_{\mathrm{u}}^{X}(\varepsilon_{11}-\varepsilon_{33}), \\ &\Delta\epsilon^{(0\,0\,1)} = \frac{2}{3}\Xi_{\mathrm{u}}^{X}(\varepsilon_{33}-\varepsilon_{11}). \end{aligned} \tag{29}$$

For [1 1 1] substrate it becomes:

$$\Delta\epsilon^{(1\,0\,0)} = \Delta\epsilon^{(0\,1\,0)} = \Delta\epsilon^{(0\,0\,1)} = 0. \tag{30}$$

Expression (30) means that for [1 1 1] substrates the X valleys remain degenerate.

Splitting of the L Valleys. For [0 0 1] substrate the splitting becomes:

$$\Delta\epsilon^{(1\,1\,1)} = \Delta\epsilon^{(\bar{1}\,1\,1)} = \Delta\epsilon^{(\bar{1}\,\bar{1}\,1)} = \Delta\epsilon^{(1\,\bar{1}\,1)} = 0. \tag{31}$$

For [1 1 0]:

$$\begin{aligned} &\Delta\epsilon^{(1\,1\,1)} = \Delta\epsilon^{(\bar{1}\,\bar{1}\,1)} = \frac{2}{3}\Xi_{\mathrm{u}}^{L}\varepsilon_{12}, \\ &\Delta\epsilon^{(\bar{1}\,1\,1)} = \Delta\epsilon^{(1\,\bar{1}\,1)} = -\frac{2}{3}\Xi_{\mathrm{u}}^{L}\varepsilon_{12}. \end{aligned} \tag{32}$$

For [1 1 1]:

$$\begin{aligned} &\Delta\epsilon^{(1\,1\,1)} = 2\Xi_{\mathrm{u}}^{L}\varepsilon_{12}, \\ &\Delta\epsilon^{(\bar{1}\,1\,1)} = \Delta\epsilon^{(\bar{1}\,\bar{1}\,1)} = \Delta\epsilon^{(1\,\bar{1}\,1)} = -\frac{2}{3}\Xi_{\mathrm{u}}^{L}\varepsilon_{12}. \end{aligned} \tag{33}$$

Expression (31) shows that the L valleys are degenerate for the substrate orientation [0 0 1]. For [1 1 0] and [1 1 1] substrates they are split. This splitting is symmetric with respect to the mean energy for the substrate oriented along [1 1 0] while it is asymmetric for the case of the substrate oriented along [1 1 1].

2.6. Effective masses in strained SiGe

To take into account effects beyond the linear deformation-potential theory the model of Rieger and Vogl [8] is used for the substrate orientation [0 0 1]. This model gives the effective masses versus Ge mole fractions in the active layer and the substrate:

$$m^*(x,y) = \begin{pmatrix} 1, & (x-y), & (x-y)^2 \end{pmatrix} \mathbf{W} \begin{pmatrix} 1 \\ (x+y) \end{pmatrix} \quad (34)$$

where $\mathbf{W}$ contains parameterized transverse and longitudinal effective masses for the perpendicular and parallel X valleys, and x and y denote the Ge mole fractions of the active layer and the substrate, respectively.

For substrate orientations different from [0 0 1] a linear interpolation

$$m^*_{\mathrm{SiGe}} = m^*_{\mathrm{Si}}(1-x) + m^*_{\mathrm{Ge}}x. \quad (35)$$

is used for the effective masses in the active layer.

3. Scattering mechanisms in strained SiGe

The changes in the band structure of strained SiGe affects the scattering processes in the active layer. These modification are discussed in the following for the main scattering processes in SiGe such as the electron–phonon and the ionized impurity scattering.

3.1. Electron–phonon scattering

The influence of strain on acoustic phonon scattering is taken into account through the modification of the number of final equivalent valleys and the final electron energy.

The final energy is given by the following expression:

$$\begin{aligned} E_{\mathrm{fin}} &= E_{\mathrm{in}} \mp \hbar\omega_{V_1V_2} + \Delta E_{ij}^{(V_1,V_2)}, \\ \Delta E_{ij}^{(V_1,V_2)} &= \Delta E_j^{(V_1)} - \Delta E_i^{(V_2)}, \end{aligned} \quad (36)$$

where $\Delta E_{ij}^{(V_1,V_2)}$ is the difference between the minima of the valleys V_1 and V_2, $V_k = X, L$ is the valley type and indices i and j denote the initial and final orientations of the valleys, respectively.

3.2. Ionized impurity scattering

The influence of strain on the Fermi level and the screening parameters of the ionized impurity scattering model [9] is considered. The effects of strain on impurity centers [10] in doped layers, however, are neglected.

For an analytical band structure taking into account nonparabolicity and anisotropy the density of states of one valley is given by

$$g(\epsilon) = \frac{\sqrt{2}m_{\mathrm{d}}^{\frac{3}{2}}\sqrt{\epsilon}}{\pi^2\hbar^3}\sqrt{1+\alpha\epsilon}\cdot(1+2\alpha\epsilon) \quad (37)$$

In order to calculate the Fermi energy in the strained material only terms up to the second order in the nonparabolicity coefficient are kept. A nonlinear equation for the Fermi energy E_{f} is obtained:

$$\begin{aligned} n = \sum_i N_{c_i}^{(\mathrm{or})} \sum_j \Big[&\mathscr{F}_{1/2}(\eta_{ij}) + \frac{15}{4}\alpha k_{\mathrm{B}} T_0 \mathscr{F}_{3/2}(\eta_{ij}) \\ &+ \frac{105}{32}\alpha^2 k_{\mathrm{B}}^2 T_0^2 \mathscr{F}_{5/2}(\eta_{ij}) \Big] \end{aligned} \quad (38)$$

where $\eta_{ij} = (E_{\mathrm{f}} - E_{c_i} - \Delta E_{c_{ij}})/k_{\mathrm{B}}T_0$, $N_{c_i}^{(\mathrm{or})}$ stands for the effective density of states of valley i with orientation j, $\Delta E_{c_{ij}}$ is the energy splitting of that valley and T_0 is the lattice temperature. The linear and quadratic terms in (38) play an important role as carriers can populate higher energy levels in highly degenerate semiconductors. (38) is solved by Newton iteration using as an initial guess the solution obtained for nondegenerate statistics and parabolic bands.

Including nonparabolicity up to the second order the contribution of valley i with orientation j to the inverse screening length takes the following form:

$$\begin{aligned} \beta_{s_{ij}}^2 = \frac{e^2}{\varepsilon_{\mathrm{s}}\varepsilon_0 k_{\mathrm{B}} T_0} N_{c_i}^{(\mathrm{or})} \cdot \Big[&\mathscr{F}_{-1/2}(\eta_{ij}) + \frac{15}{4}\alpha k_{\mathrm{B}} T_0 \cdot \mathscr{F}_{1/2}(\eta_{ij}) \\ &+ \frac{105}{32}\alpha^2 k_{\mathrm{B}}^2 T_0^2 \cdot \mathscr{F}_{3/2}(\eta_{ij}) \Big], \end{aligned} \quad (39)$$

It should be noted that in semiconductors with nonparabolic bands the inverse screening length increases which may weaken the ionized impurity scattering rate in particular for a high doping level when due to the Pauli exclusion principle the population of higher energies increases significantly. Thus there are two opposite factors which determine the strength of ionized impurity scattering. Another interesting effect occurs in strained doped materials. Due to strain some valleys shift up and do not contribute to the kinetics. However, this may change at high degeneracy when the Pauli principle causes the upper split bands to be populated, which then also give a contribution to the transport properties. The repopulation may be significant leading to a reduction of the valley splitting effect.

In case of momentum-dependent screening the dielectric function is modified to take into account the strain induced splitting of the conduction band minima for different valleys and orientations:

$$\varepsilon(q) = \varepsilon(0) \cdot \left(1 + \frac{1}{q^2} \sum_{ij} \beta_{s_{ij}}^2 G_{ij}(\xi, \eta_{ij}) \right), \quad (40)$$

where G_{ij} stands for the screening function in valley i with orientation j. The momentum transfer $\mathbf{q} = \mathbf{k}' - \mathbf{k}$ and the temperature dependence enters through ξ:

$$\xi^2 = \frac{\hbar^2 q^2}{8m^* k_B T_L}. \tag{41}$$

4. Zero field Monte Carlo method

In this work we use a Monte Carlo algorithm for zero electric field and degenerate statistics [11,12]. The Pauli exclusion principle is taken into consideration in the scattering term of the Boltzmann equation. As a result the Boltzmann equation becomes nonlinear.

As a starting point we use the transient Boltzmann transport equation with a scattering operator including the Pauli blocking factor. As we only consider bulk semiconductors, the space dependence of the distribution function and the differential scattering rates is neglected. We also suppose the scattering rate to be time invariant.

After linearization and transformation of the Boltzmann equation to integral form [14] and assuming an impulse-like excitation for the electric field, we derive the following equation for the perturbation $f_1(\mathbf{k}, t)$ of the distribution function:

$$\begin{aligned} f_1(\mathbf{k},t) = {} & \int_0^t \mathrm{d}t' \int \mathrm{d}\mathbf{k}' f_1(\mathbf{k}',t') \cdot \widetilde{S}\left(\mathbf{k}',\mathbf{K}(t')\right) \\ & \cdot \exp\left[-\int_{t'}^t \tilde{\lambda}(\mathbf{K}(y))\,\mathrm{d}y\right] \\ & + G(\mathbf{K}(0)) \cdot \exp\left[-\int_0^t \tilde{\lambda}(\mathbf{K}(y))\,\mathrm{d}y\right]. \end{aligned} \tag{42}$$

The differential scattering rate $\widetilde{S}(\mathbf{k}', \mathbf{k})$ and the total scattering rate $\tilde{\lambda}(\mathbf{k})$ are defined by the following expressions:

$$\begin{aligned} \widetilde{S}(\mathbf{k}',\mathbf{k}) &= [1 - f_s(\mathbf{k})] \cdot S(\mathbf{k}',\mathbf{k}) + f_s(\mathbf{k}) \cdot S(\mathbf{k},\mathbf{k}') \\ \tilde{\lambda}(\mathbf{k}) &= \int \widetilde{S}(\mathbf{k},\mathbf{k}')\,\mathrm{d}\mathbf{k}', \end{aligned} \tag{43}$$

where $f_s(\mathbf{k})$ is the stationary distribution function, $S(\mathbf{k}', \mathbf{k})\,\mathrm{d}\mathbf{k}'$ is the scattering rate from $\mathrm{d}\mathbf{k}'$ to a state with wave vector $\mathbf{k}$, which must not be occupied. Employing the δ-function of the Fermi golden rule the expression for $\tilde{\lambda}(\mathbf{k})$ can be rewritten in the following manner:

$$\tilde{\lambda}(\mathbf{k}) = [1 - f_s(\epsilon_f)] \cdot \lambda(\mathbf{k}) + f_s(\epsilon_f) \cdot \lambda^*(\mathbf{k}), \tag{44}$$

where ϵ_f is the final energy, $\lambda(\mathbf{k}) = \int S(\mathbf{k}, \mathbf{k}')\,\mathrm{d}\mathbf{k}'$ is the total scattering rate, $\lambda^*(\mathbf{k}) = \int S(\mathbf{k}', \mathbf{k})\mathrm{d}\mathbf{k}'$ is the total backward scattering rate. The new variables $\widetilde{S}(\mathbf{k}', \mathbf{k})$ and $\tilde{\lambda}(\mathbf{k})$ introduced above are used to construct the Monte Carlo algorithm. It should be also noted that for non-degenerate statistics ($f_s \ll 1$) this algorithm gives the method described previously [13]. For intermediate doping levels (44) describes a linear combination of the total scattering rate $\lambda(\mathbf{k})$ and the backward scattering rate $\lambda^*(\mathbf{k})$, while for the degenerate case ($f_s \lesssim 1$) the kinetic properties are predominantly determined by the backward scattering rate $\lambda^*(\mathbf{k})$.

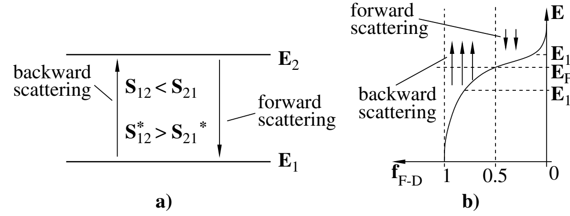

Fig. 4. Schematic illustration of the scattering processes at high degeneracy.

Since at high doping levels the backward scattering rate is dominant, the probability to scatter to higher energy states is larger than to lower energy states, as schematically shown in Fig. 4(a). This means that lower energy levels are already occupied by particles (see Fig. 4(b)) and, due to the Pauli exclusion principle, scattering to these energy levels is quantum mechanically forbidden.

The mobility component μ_{ij} is computed by the following algorithm:

1. Set $n = 0$, $w = 0$.
2. Select initial state $\mathbf{k}$ arbitrarily.
3. Compute a sum of weights:

   $w = w + [1 - f_{FD}(\epsilon)][v_j(\mathbf{k})/\tilde{\lambda}(\mathbf{k})]$.
4. Select a free-flight time $\tilde{t}_f = -\ln(r)/\tilde{\lambda}(\mathbf{k})$ and add time integral to estimator: $n = n + wv_i\tilde{t}_f$ or use the expected value of the time integral: $n = n + wv_i/\tilde{\lambda}(\mathbf{k})$.
5. Perform scattering. If the scattering mechanism was isotropic, reset weight: $w = 0$.
6. Continue with step 3 until N $\mathbf{k}$-points have been generated.
7. Calculate component of zero field mobility tensor as $\mu_{ij} = q\langle\tilde{\lambda}\rangle n/(k_B T_0 N)$.

5. Simulation results

Results of Monte Carlo simulations of strained SiGe layers are presented. First the low field electron mobility is investigated as a function of the Ge compositions of both the active layer and the substrate for the undoped case. Then strained doped layers are studied. Finally, the influence of the substrate orientation is demonstrated. All results are presented for room temperature.

Fig. 5 shows $\mu_\perp$, the electron mobility perpendicular to the interface for several substrate orientations, while Fig. 6 demonstrates $\mu_\parallel$, the electron mobility parallel to the interface for the same substrate orientations. Figs. 7 and 8 show the population of the X and L valleys for

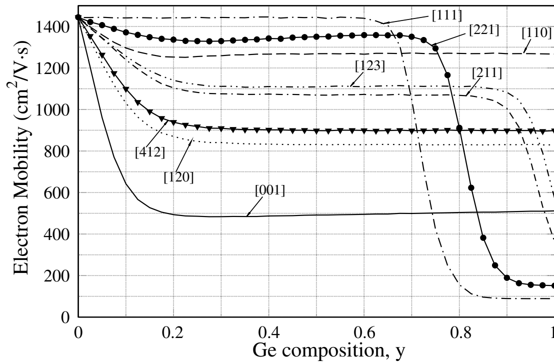

Fig. 5. Perpendicular component of the low field electron mobility $\mu_\perp$.

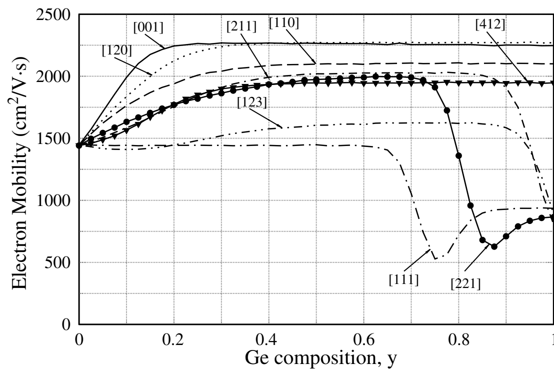

Fig. 6. In-plane component of the low field electron mobility $\mu_\parallel$.

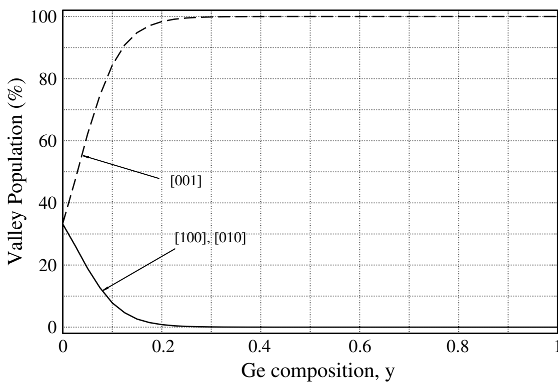

Fig. 7. Valley population for the substrate orientation [0 0 1].

different orientations. As it is seen from Fig. 7, the X valleys with orientations [1 0 0] and [0 1 0] are not split in accordance with (29). The L valleys remain unpopulated in this case as they are much higher than the X valleys. The decrease of $\mu_\perp$ and increase of $\mu_\parallel$ is explained by the

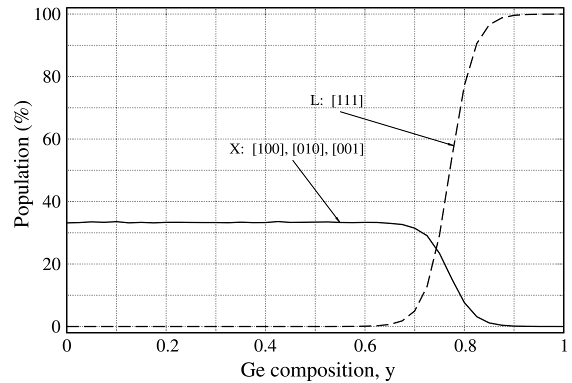

Fig. 8. Valley population for the substrate orientation [1 1 1].

population of the X valleys with orientation [0 0 1] which contribute through m_t^X to the in-plane and m_l^X to the perpendicular transport. Fig. 8 provides an explanation of the mobility components for the substrate orientation [1 1 1]. The X valleys are not split in accordance with (30). When the Ge composition in the substrate increases, the splitting of the L valleys becomes important. The valleys with orientations $[\bar{1}\,1\,1]$, $[\bar{1}\,\bar{1}\,1]$ and $[1\,\bar{1}\,1]$ go up and remain empty while the L valley oriented along [1 1 1] goes strongly down as stated by (33). This valley is dominant at high Ge mole fractions. Now the in-plane and perpendicular transport is determined by m_t^L and m_l^L respectively. The increase of $\mu_\parallel$ at high compositions y is related to the decrease of the $X \rightarrow L$ intervalley transitions. $\mu_\perp$ does not increase due to the higher value of m_l^L. The range of Ge compositions where the $X \rightarrow L$ transitions are most effective can be seen in Fig. 9, showing the band edges versus the substrate composition y.

Fig. 10 shows the dependence of $\mu_\parallel$ on the in-plane angle given by the third Euler angle γ for [1 1 0] substrate orientation. For substrates with a general orientation the mobility becomes anisotropic. This means that the in-plane mobility depends on the orientation of the de-

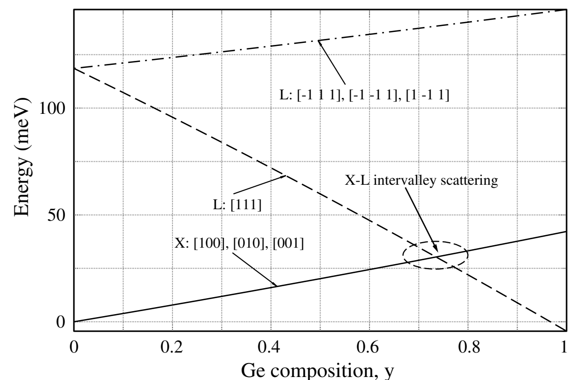

Fig. 9. Band edges in the active layer grown on the substrate with the orientation [1 1 1].

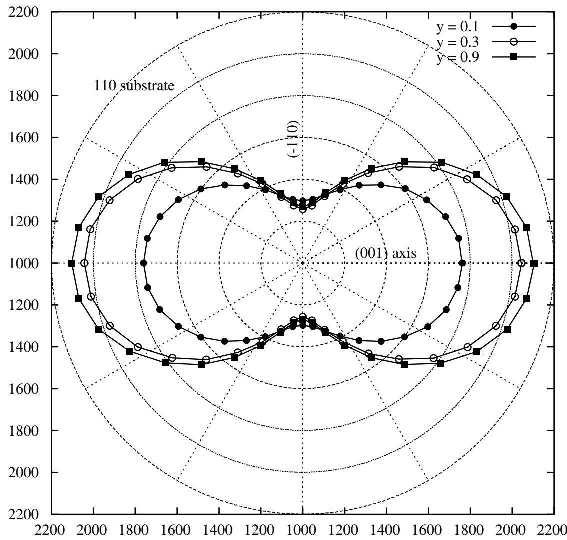

Fig. 10. In-plane electron mobility $\mu_{\|}$ (cm^2/V s) as a function of γ in Si grown on [1 1 0] $Si_{1-y}Ge_y$.

vices built in the substrate. Thus in order to reach optimal characteristics the active strained regions of a device has to be properly oriented on the surface of the substrate.

In Fig. 11 the low field electron mobility in undoped $Si_{1-x}Ge_x$ layers is given. The essential difference in comparison with Si layers is that now alloy scattering strongly influences the transport properties. Alloy scattering as a function of the Ge composition x in the active layer has its maximum at $x = 0.5$. Therefore one might expect that electron mobility has its minimum at the same point. However, both the change of the effective masses and repopulation effects between valleys, both of the same and different types, can be strong enough to suppress the decrease of the electron mobility due to alloy scattering.

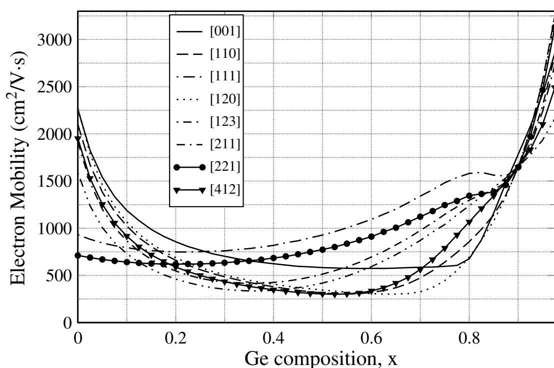

Fig. 11. In-plane electron mobility $\mu_{\|}$ in $Si_{1-x}Ge_x$ on $Si_{0.1}Ge_{0.9}$ for several substrate orientations.

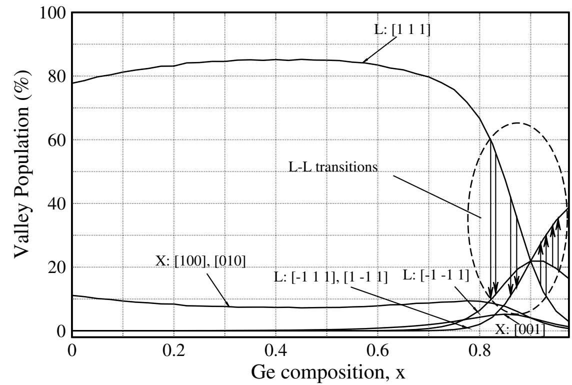

Fig. 12. Valley populations as functions of the active layer composition for the $Si_{0.1}Ge_{0.9}$ substrate with orientation [2 2 1].

The in-plane components $\mu_{\|}$ of the electron low field mobility are presented in Fig. 11 as functions of the layer composition x for several substrate orientations. The Miller indices specify only two Euler angles α and β while the third Euler angle γ is assumed to be zero. Fig. 12 explains the behavior of the mobility components for a $Si_{0.1}Ge_{0.9}$ substrate oriented along [2 2 1]. It shows the populations of the X and L valleys with different orientations. The L valley oriented along [1 1 1] is highly populated up to $x \approx 0.8$ and thus the contribution of the longitudinal effective masses of the L valley plays the main role. This reduces the mobility components $\mu_{\perp}$ and $\mu_{\|}$. The increase of the in-plane component $\mu_{\|}$ is related to the composition dependence of the effective masses. When the Ge mole fraction is greater than $x = 0.8$, a repopulation between different L valleys occurs. First electrons scatter from the valley located along [1 1 1] to the valleys located along $[\bar{1}\,1\,1]$, $[1\,\bar{1}\,1]$ and $[\bar{1}\,\bar{1}\,1]$ and then from [1 1 1] and $[\bar{1}\,\bar{1}\,1]$ to $[\bar{1}\,1\,1]$, $[1\,\bar{1}\,1]$. In this way the influence of the longitudinal masses reduces while the transverse masses contribute more and more leading to the rapid mobility increase at higher values of the Ge mole fraction.

Figs. 13 and 14 demonstrate the doping dependence of $\mu_{\perp}$ and $\mu_{\|}$ in the Si active layer grown on a relaxed $Si_{0.1}Ge_{0.9}$ substrate. In Fig. 13 the curve for the perpendicular component $\mu_{\perp}$ exhibits an increase for the [0 0 1] substrate when the doping level becomes high enough. At the same time the in-plane component does not increase as shown in Fig. 14. This effect can be explained by the influence of the Pauli exclusion principle which starts playing an important role at high doping level. At low doping level the L valley oriented along [1 1 1] is the lowest one. Its population is equal to 100% (see Fig. 15) and $\mu_{\perp}$ is determined by m_l^L, while $\mu_{\|}$ is determined by m_t^L. As the donor concentration increases, scattering to lower energy levels is forbidden by the Pauli exclusion principle and thus electrons scatter to

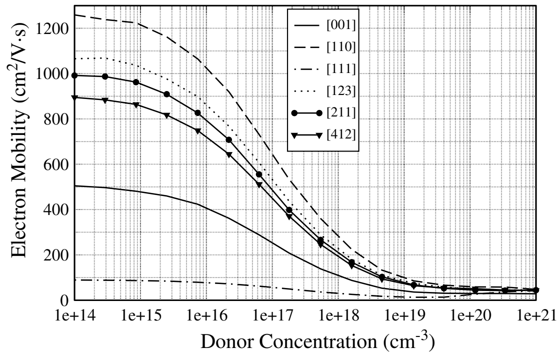

Fig. 13. Doping dependence of $\mu_{\perp}$ in Si on $Si_{0.1}Ge_{0.9}$.

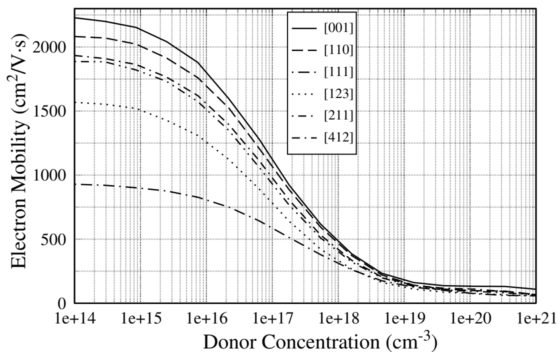

Fig. 14. Doping dependence of $\mu_{\|}$ in Si on $Si_{0.1}Ge_{0.9}$.

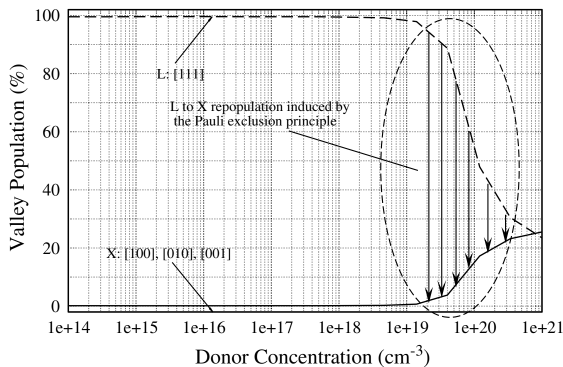

Fig. 15. Valley population in strained Si grown on the $Si_{0.1}Ge_{0.9}$ substrate oriented along [1 1 1].

higher energy levels. At doping level about 10^{19} cm^{-3} electrons occupy energies high enough to allow for scattering to the unsplit X valleys which due to strain effects lie higher than the L valleys. Intervalley $L-X$ scattering becomes possible and gets stronger as the donor concentration increases. Finally, electrons are almost equally distributed among the X valleys. The influence of m_l^L on $\mu_{\perp}$ is significantly reduced and this turns out to be enough to suppress the increasing ionized impurity scattering. However, the X valleys are oriented such that the influence of m_l^X and m_t^X on $\mu_{\|}$ is not so strong to suppress the impurity scattering and as a result $\mu_{\|}$ does not show an increase.

6. Conclusion

The behavior of the low field electron mobility in strained $Si_{1-x}Ge_x$ layers grown on relaxed $Si_{1-y}Ge_y$ substrates as a function of x, y and the orientation of the substrate has been analyzed using a Monte Carlo approach. The strain effects have been treated in the linear deformation-potential formalism applied to the X and L valleys of the conduction band. The influence of the conduction band minima splitting on the scattering processes has been taken into account. A zero field Monte Carlo method has been applied to solve the nonlinear Boltzmann kinetic equation accounting for the Pauli exclusion principle. Results obtained for the electron mobility in strained layers have been discussed for undoped and doped layers and arbitrarily oriented substrates. The dependences on the Ge compositions x and y and the donor concentration have been demonstrated. The population of the conduction band minima has been studied to explain the influence of the Pauli exclusion principle in the strained material. The dependence of the mobility on the in-plane angle has been demonstrated. A pronounced anisotropy is observed.

Acknowledgements

This work has been partly supported by the Semiconductor Research Corporation (SRC), project number 998.001.

References

[1] Fischetti MV, Laux SE. J Appl Phys 1996;80:2234.
[2] Bufler FM, Graf P, Keith S, Meinerzhagen B. Appl Phys Lett 1997;70:2144.
[3] Jacoboni C, Reggiani L. Rev Mod Phys 1983;55:645.
[4] Bardeen J, Shockley W. Phys Rev 1950;80:72.
[5] Ridley BK. Quantum processes in semiconductors. New York: Oxford University Press; 1993.
[6] Balslev I. Phys Rev 1966;143:636.
[7] Ferry DK. Semiconductors. New York: Macmillan; 1991.
[8] Rieger MM, Vogl P. Phys Rev B 1993;48:14276.
[9] Kosina H, Kaiblinger-Grujin G. Solid-State Electron 1998;42:3096.
[10] Bir GL, Pikus GE. Symmetry and strain-induced effects in semiconductors. New York: John Wiley; 1974.

[11] Smirnov S, Kosina H, Nedjalkov M, Selberherr S. Large-scale scientific computing, Sozopol, Bulgaria. Berlin: Springer; 2004. p. 185–93.
[12] Smirnov S, Kosina H, Nedjalkov M, Selberherr S. J Appl Phys 2003;94:5791.
[13] Kosina H, Nedjalkov M, Selberherr S. Large-scale scientific computing, Sozopol, Bulgaria. Berlin: Springer; 2001. pp. 175–82.
[14] Kosina H, Nedjalkov M, Selberherr S. IEEE Trans Electron Dev 2000;47:1898.